

THE INTERNATIONAL SOCIETY OF  
PRECISION AGRICULTURE PRESENTS THE  
13<sup>th</sup> INTERNATIONAL CONFERENCE ON  
**PRECISION AGRICULTURE**

July 31-August 4, 2016 • St. Louis, Missouri USA

## Selection and Utility of Uncooled Thermal Cameras for Spatial Crop Temperature Measurement within Precision Agriculture

D. L. Mangus, A. Sharda

Biological and Agricultural Engineering, Kansas State University, 129 Seaton Hall,  
Manhattan, KS 66506. Email: [deman@ksu.edu](mailto:deman@ksu.edu) ; [asharda@ksu.edu](mailto:asharda@ksu.edu)

A paper from the Proceedings of the  
13<sup>th</sup> International Conference on Precision Agriculture  
July 31 – August 4, 2016  
St. Louis, Missouri, USA

**Abstract.** Since previous research used local, single-point measurements to indicate crop water stress, thermography is presented as a technique capable of measuring spatial temperatures supporting its use for monitoring crop water stress. This study investigated measurement accuracy of uncooled thermal cameras under strict environmental conditions, developed hardware and software to implement uncooled thermal cameras and quantified intrinsic properties that impact measurement accuracy and repeatability. A DRS Tamarisk® 320 (CAM1) and FLIR® Tau 2 (CAM2) were selected for this study. Results indicated that wide and medium angle lens distortion was 19% for CAM1 and 30% for CAM2. A minimum of four pixels were recommended to maintain surface temperature integrity and maximize image coverage area. A 19 and 7 min warm-up was necessary for CAM1 and CAM2 respectively. A real-time (RT) and one-time (OT) radiometric calibration provided absolute surface temperatures with environmental compensation. CAM1 analog output yielded a configurable temperature span from 5°C-156°C, resolution from 0.02°C-0.61°C, and measurement accuracy of  $\pm 0.82^\circ\text{C}$  or  $0.62^\circ\text{C}$  with OT or RT radiometric calibration, respectively, whereas digital output yielded a fixed temperature span of 156°C, resolution of 0.01°C and measurement accuracy of  $\pm 0.43$  or  $0.29^\circ\text{C}$  with OT or RT radiometric calibration, respectively. CAM2 yielded a controllable temperature span of 18°C-206°C, resolution of 0.07°C-0.80°C, and measurement accuracy of  $\pm 0.87$  or  $0.63^\circ\text{C}$  with OT or RT radiometric calibration, respectively. Both cameras were sensitive to surface temperatures ( $R^2=0.99$ ); but, CAM1 was more controllable. Results highlight that uncooled thermal cameras can measure spatial temperatures, thereby measuring subtle crop dynamics for water resource management.

**Keywords:** thermography, remote sensing, environmental influence, imagery, thermal infrared, sUAS, uncooled thermal camera.

### Introduction

In the midst of recent droughts, increased water demand, and the implementation of water allocations for conservation, irrigated acreage throughout the United States increased by nearly 1.3 million acres from 2002 to 2007 (USDA, 2014). The largest percentage of irrigated farms is located in the western United States where competition for irrigation water availability has escalated in the past two decades (Taghaeian, et al., 2013). In the Midwest, for example, average irrigated corn yield has increased approximately 2.5 bushels per acre per year since the early 1970s. Diminishing irrigation water requires efficient water management practices using monitoring

and control for sustainable water management (Adeuya, 2007). Other water conservation projects have developed smart-water systems that use less water from aquifers and above-ground freshwater sources while investigating soil-improving strategies in which drought-tolerant crop varieties are chosen according to a climate's available water (Berton, 2006). Although these and other advances in precision irrigation technologies are becoming available to producers, adoption of these systems for commercial applications requires producers to monitor crop water stress at increased spatial (ground sample distance (e.g., 1 cm/pixel)) and temporal (revisit frequency) resolution.

Research shows that crop growth and yield are directly affected by water stress but only partially affected by soil-water interaction (Zhang & Kovacs, 2012). Current irrigation schedules are typically based on soil moisture deficits; however, localized soil moisture sensors are not representative of spatial moisture variability that may exist throughout the field. As a result, direct measurement of canopy temperatures with manual or mounted infrared thermometers (IRTs) on pivot systems have been used to quantify crop water stress because plants close their leaf stomata under periods of water stress, thereby reducing transpiration and causing proportionally increased leaf temperatures (Evans, et al., 2000).

Although irrigation scheduling has used canopy temperature and soil moisture monitoring, these tedious and time-consuming methods yield limited samples at less resolution than is required to perform precision irrigation, consequently proving the methods to be impractical for commercial applications (Jones, 2004). While an IRT can take quick measurements, a thermal infrared imaging system (TIRIS) can monitor multiple crop profiles per image. This novice, less studied technology can monitor spatial crop temperatures in irrigation applications and in periods of drought, weed infestation, heat tolerant phenotype trait expression, and herbicide and nutrient applications. Limited publications describe United States studies of thermal infrared (TIR) cameras for measuring crop temperature profiles, specifically crops whose yield significantly increases with irrigation in the water-stressed Midwest.

Increased interest among United States agricultural producers regarding small unmanned aerial systems (sUAS) allows possibility for a TIRIS designed for lightweight, high-throughput sensing that could measure crop temperature variability and assess spatial crop water stress in agricultural production. However, available knowledge regarding thermal sensing platform performance in agricultural field studies is limited, and producers are skeptical of technology that has demonstrated potential for measuring crop temperature profiles and enabling site-specific water management in orchards, vineyards, and other specialty crops in areas outside of the United States (Sepulcre-Canto, et al., 2011). Lack of knowledge can be attributed to the expense of cooled TIR cameras which has made crop temperature measurements in commercial agriculture economically unfeasible. However, innovation of the uncooled thermal sensor has led to development of new, lightweight TIR cameras that have no moving parts and require no cooling package, thereby providing extended operating life at a fraction of the cost of previous cooled TIR cameras.

Because microbolometer thermal detectors are uncooled, they have a low signal-to-noise ratio, the amount of usable signal compared to noise signal. Consequently, uncooled TIR detectors are less accurate ( $\pm 0.1^{\circ}\text{C}$ ) than other temperature sensors (Kuenzer, 2014); however, this accuracy, also known as sensor measurement confidence, make microbolometers' sensitive to subtle temperature differences ( $< 0.5^{\circ}\text{C}$ ) necessary for accurate crop health stress assessment (Blonquist & Bugbee, n.d.; Sepulcre-Canto, et al., 2007). In agricultural and environmental studies, natural objects have been found to emit long wave infrared (LWIR) radiation, a region of 7 to 14  $\mu\text{m}$  wavelength bandwidth ( $-66.2^{\circ}\text{C}$  to  $140.0^{\circ}\text{C}$ ). Microbolometer image sensors are sensitive to LWIR radiation that strikes the detector material, changing the detectors' electrical resistance from a change in temperature, thereby transforming temperature intensity into a raw digital value (DV) generating a thermal image (Kuenzer, 2014).

Internal circuitry heat and external temperature exposure require uncooled TIR cameras to regulate their microbolometer sensors with automatic temperature recalibration. Consequently, TIR camera warm-up time can alter measurement accuracy (i.e., closeness to the true value) by microbolometer recalibration thereby requiring warm-up periods in order to reach a steady-state operating temperature (Figure 1).

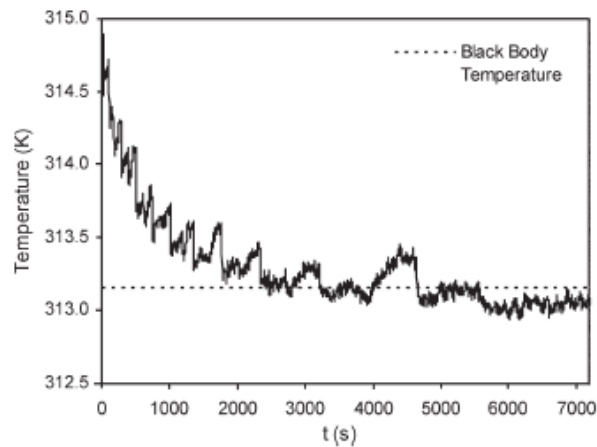


Figure 1. Changes of radiometric temperature measured by TIR camera during warm-up period. Adapted from Berni et al. (2009).

As shown in Figure 1, Berni et al. (2009) studied a TIR camera with a recommended warm-up period of 2 h before the measured temperature converged to a steady-state blackbody (i.e., object or system that absorbs and emits electromagnetic radiation equal to its internal kinetic temperature (Kuenzer, 2014)) temperature. As a result, limited literature exists testing uncooled TIR cameras in order to create standard operating protocols under practical scenarios.

For a camera, the sensed object and desired sensing distance determines the choice of lens (Elfaki, et al., 2000). Maintained focus over a wide range of temperatures is essential for system performance, stability, and imaging quality. An athermalized lens maintains performance using optical passivity over the sensitive temperature span. Unlike typical visible cameras, the TIR camera lens focal length may need to be adjusted to focus on particular sensing distances (DRS Technologies A Finmeccanica Company, 2013). However, TIR camera lenses are subject to the same geometric calibration parameters as visible imagery including focal distance, point coordinates, and radial distortion (Berni, et al., 2009; Kuenzer, 2014). Because thermal radiation does not transfer through glass, TIR camera lenses are made from germanium that allows the transmission of TIR radiation (Kuenzer, 2014). Germanium lenses are optimized for radiant heat transmission, consequently making them more susceptible to geometric distortion. According to Lagueta et al. (2013), increased lens distortion is more common for TIR cameras compared to glass lenses because of their short focal length and germanium material.

Expectations associated with TIRIS rely on accurate temperature measurement, high imaging speed, limited image noise, and optimized storage of raw images. This research will support future studies to develop a full system package for capturing accurate spatial canopy temperatures aboard sUAS and ground-based sensing platforms in order to create high definition canopy temperature maps and aid variable rate irrigation decision management. As stated, increased irrigated acres in the Midwest depend primarily on declining fresh water reserves. Significant studies have indicated that a very high level of management is required in order to maintain or improve irrigation water productivity and economic return with decreasing water resources. Researchers, TIR and sUAS manufacturers, agricultural service providers, and producers in the Midwest are eager to adopt thermal technologies in precision agriculture, such as a TIRIS aboard sUAS and ground-based platforms to assist with efficient and accurate water utilization. Therefore, this study investigated industry-leading TIR camera cores under strict laboratory conditions (i.e., air temperature, relative humidity, incident radiant heat) to determine measurement accuracy under anticipated field conditions. In addition to thermography potential, **core objectives of this research were to** (1) quantify measurement accuracy and intrinsic properties of two commercially available uncooled TIR camera cores, (2) investigate impact of physical properties and environmental conditions on measurement accuracy, and (3) determine necessary equipment and considerations when integrating an uncooled TIR camera core into a TIRIS for accurate crop temperature measurement.

## Methods and Materials

Strict laboratory experiments were conducted at the Department of Biological and Agricultural Engineering at Kansas State University, Manhattan, Kansas. A DRS Tamarisk® 320 (DRS Technologies, Inc., Dallas, Texas) and FLIR® Tau 2-324 (FLIR® Systems, Inc., Boston, Massachusetts), hereafter referred as CAM1 and CAM2, were studied to benchmark their utility in precision agriculture. These cameras were selected because of their minimal size, lightweight design, and limited power consumption. Utility was investigated with regards to integration hardware and software, camera controllability for changing applications, and radiometric measurement accuracies. CAM1 was further investigated to determine environmental conditions that impact temperature measurement.

## Determining Physical Properties of TIR Camera

Cameras have physical parts and capabilities that influence their sensitivity to temperature differences, increase their measurement error, and limit their use in agricultural environments. Due to their relatively low cost compared to cooled thermal cameras, minimal size and weight, and no moving parts, uncooled TIR cameras provide increased coverage area and crop stress assessments aboard different sensing platforms not possible with cooled TIR cameras and IRTs. The identified physical properties that restrict practical use of TIR cameras include:

1. *Lens selection and distortion*
2. *Image resolution and measurement*
3. *Radiometric characterization and measurement accuracy*
4. *Warm-up time and automatic recalibration*
5. *Connection ease, software, and controllability*

Considering these physical properties and their influence on accurate measurement may allow for their influence to be reduced or eliminated with proper camera configuration, hardware, standard operating protocol, and sensing platform. Therefore, intrinsic fundamentals of uncooled TIR cameras were investigated using the methods discussed in the following sections.

### *Lens Selection and Distortion*

Lens selection was investigated because specific target size and sensing distance determines the lens and resulting image size for a specific application. TIR cameras have germanium lenses that are factory-installed and calibrated, consequently increasing the cost of additional lenses and requiring expensive equipment for recalibration. Due to the small lens focal length, both TIR camera lens distortions were investigated in order to correct lens distortion for spatial integrity. A distorted image does not fully represent real spatial points but a distorted location dependent on the position within the lens' field of view (FOV). CAM1 features an 11 mm, medium angle lens with a  $27^{\circ} \times 20^{\circ}$  degree angle FOV and CAM2 features a 7.5 mm, wide angle lens with a  $63^{\circ} \times 50^{\circ}$  degree angle FOV. Using a distortion model (grid) calibration approach (Sun, et al., 2013), each TIR camera lens distortion was corrected based on multiple calibration grid images using a heated grid pattern tool. The grid distortion model required at least five images from different orientations in order to calibrate radial and tangential distortion coefficients. Thermal images were imported into the NI LabVIEW™ Vision Assistant (National Instruments Corporation, Austin, Texas) for lens distortion analysis.

### *Image Resolution and Measurement*

Since TIR cameras typically have lower resolution image sensors than visible cameras, the target size and sensing distance is more critical when determining the lens focal length (distance from the lens to the thermal detector) and resulting FOV degree angle. Critical pixel resolution was investigated by using a known target size and determining the necessary number of incident pixels in order to limit inaccuracies. A target measuring 16 mm in diameter was heated and placed on a flat surface at a stable temperature for TIR camera visibility (Figure 2).

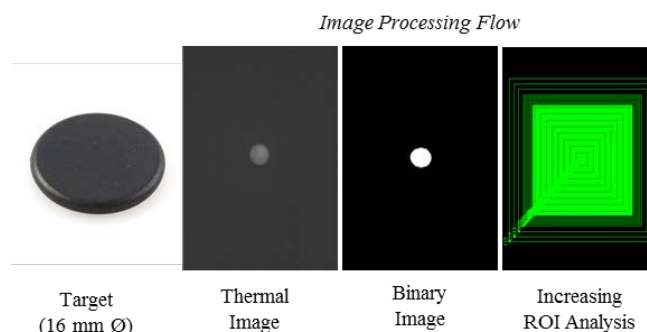


**Figure 2. Investigation of necessary spatial resolution for temperature accuracy**

As shown in Figure 2, the thermal image was altered into a binary image (i.e., white=1 | black=0) in order to maximize the contrast between the accurate and inaccurate measured value of 1 and 0, respectively. As the last image processing step, a series of increasing regions of interest (ROI) were designated by increasing the offset pixel resolution by 1 pixel (i.e.,  $1 \times 1$ ,  $3 \times 3$ ,  $5 \times 5$ ,  $7 \times 7$ , ...,  $333 \times 333$  pixel resolution) centered directly over the target. Increasing the spatial resolution by 1 pixel (or 0.33 mm/pixel) around the outer perimeter for each subsequent ROI allowed the average DV to be calculated with the LabVIEW™ Vision Assistant™.

## Radiometric Characterization and Measurement Accuracy

Uncooled TIR cameras measure LWIR energy intensity present on the image sensor, thereby generating a thermal image of radiated surface temperatures. CAM1 is sensitive to 8 to 14  $\mu\text{m}$  LWIR, or a theoretical temperature span from  $-66^{\circ}\text{C}$  to  $90^{\circ}\text{C}$  ( $\sim\Delta 156^{\circ}\text{C}$ ), while CAM2 is sensitive to 7 to 14  $\mu\text{m}$  LWIR, or a theoretical temperature span from  $-66^{\circ}\text{C}$  to  $140^{\circ}\text{C}$  ( $\sim\Delta 206^{\circ}\text{C}$ ). However, the uncooled TIR camera cores only measure relative temperature values, leaving temperature measurements unquantified. Therefore, a calibration method was developed to characterize pixel intensity-to-actual temperature using reference temperature panels viewable within a camera's FOV in order to create a radiometric calibration transfer function. A near-perfect blackbody enclosure, hereafter termed as "BB enclosure", was built from wood and painted flat black to isolate the camera and target surfaces from outside influences while investigating this radiometric calibration method (Figure 3).

Three reference surfaces were used to provide temperature differentials necessary for the radiometric calibration (Figure 3 c). An isolated  $0.10\times 0.10$  m piece of 8 mm thick wood, painted flat black, was used as a box reference that fluctuated with ambient air temperature. A  $0.30\times 0.60$  m piece of 1.52 mm thick (14 gauge) aluminum sheet metal was fabricated for use as the heated target surface. An electric heating element in the BB enclosure was capable of heating the aluminum panel up to  $65^{\circ}\text{C}$  at a manual or automatic rate determined by the BB enclosure heating element and air exchange vent controller. The third reference panel is identified as the wet reference. To make the wet reference, a highly evaporative cloth (Chilly Padd, Arab, Alabama) was placed around a solid wooden dowel and placed in a bottle of water for continuous wicking and evaporation, thereby creating a stable, cool reference temperature.

For apparent temperature correction, a commercial IRT (Fluke 62 MAX, Fluke Corporation, Everett, Washington) with a measurement accuracy of  $\pm 1^{\circ}\text{C}$  and an adjustable emissivity correction from 0.1 to 1 was used to determine the emissivity of the reference targets. To determine emissivity, surface temperatures measured with the IRT were corrected to match actual surface temperatures measured with the thermistors. Emissivities of 0.82, 0.88, and 0.96 were found for the flat-black painted wooden box and aluminum panel and wet reference, respectively.

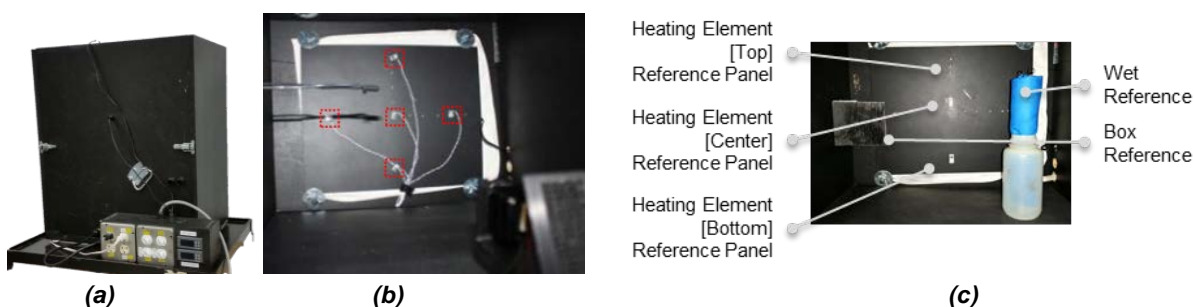


**Figure 3. (a) BB enclosure constructed to limit outside influence. (b) Surface mount thermistors measured actual target surface temperatures within an ROI (shown in red) to characterize pixel intensities. (c) Heating element, box reference equal to air temperature and a cool, wet reference.**

In addition to controlling the heating element, the BB enclosure regulates air exchange within the chamber until set air conditions are automatically or manually reached to determine the environmental influence as described in Section 2.3.2, below. Actual surface temperatures were measured with five surface-mounted thermistors (ON-930-44033, OMEGA, Stamford, Connecticut) with a measurement accuracy of  $\pm 0.1^{\circ}\text{C}$ . In addition, a surface-mount thermistor was attached to the camera housing to monitor operating camera housing temperatures during TIR camera evaluations.

Relative humidity and air temperature within the BB enclosure were measured with a combination sensor (Omega Engineering Inc., Stamford, Connecticut) with an accuracy of  $\pm 3\%$  and  $\pm 0.2^{\circ}\text{C}$ , respectively. A data acquisition system was built using a NI myRIO (National Instruments Corporation, Austin, Texas) to monitor the surface mount thermistors, air temperature, and relative humidity inputs from sensors within the BB enclosure. A TIR Camera Evaluation Software program was developed using NI LabVIEW™ (National Instruments Corporation, Austin, Texas) to acquire real-time image data, camera housing temperature, actual reference surface temperatures, air temperature, and relative humidity while controlling test length and file specifications. Raw data was monitored at a sampling frequency of 9 Hz to match the frame rate of the TIR camera cores.

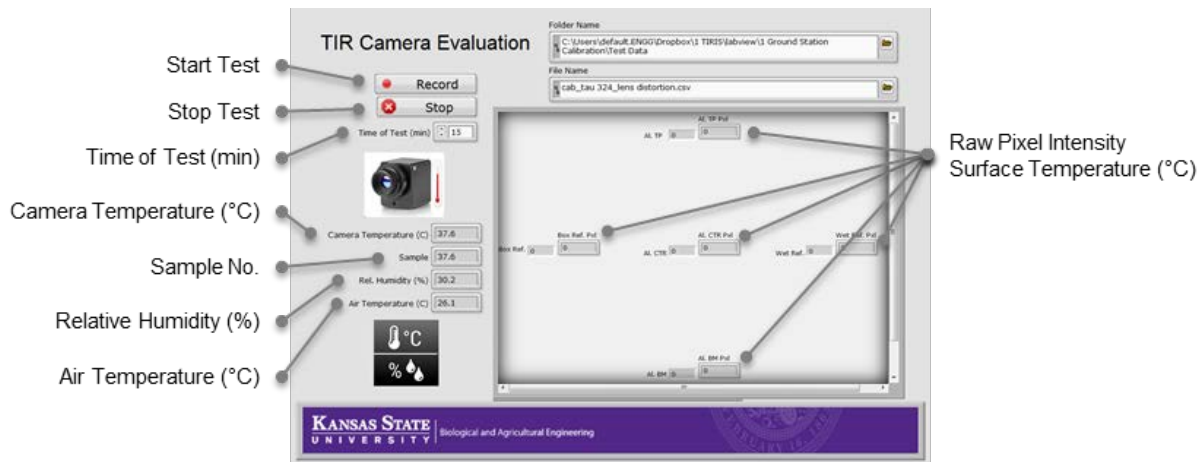


Figure 4. TIR Camera Evaluation Software VI used to conduct radiometric calibrations while recording raw data.

The TIR Camera Evaluation Software program averaged multiple image pixels within static ROIs within the TIR camera FOV to correlate pixel intensity-to-actual surface temperature (Figure 4, above). Raw pixel intensities ( $X_1$ ,  $X_2$ ) were combined with actual surface temperature ( $Y_1$ ,  $Y_2$ ) to determine the radiometric transfer function slope, as defined by Equation 1:

$$m = \frac{Y_2 - Y_1}{X_2 - X_1} \quad (1)$$

By using the slope found in Equation 2.3 and a raw pixel and coinciding surface temperature ( $X_1$ ,  $Y_1$ ), the y-intercept of the radiometric transfer function was determined using Equation 2:

$$Y - Y_1 = m(X - X_1) \quad (2)$$

When a radiometric transfer function was found, each digital image pixel was converted to a temperature value defined by Equation 3:

$$T_{(i,j)} = T_{min} + \frac{I_{(i,j)}}{2^N - 1} T_{span} \quad (3)$$

here:

- $T_{(i,j)}$  = Pixel temperature (°C) at row  $i$  and column  $j$ ,
- $T_{min}$  = Lowest temperature within the image (°C),
- $I_{(i,j)}$  = Pixel intensity at row  $i$  and column  $j$ ,
- $N$  = Number of bits for pixel intensity (e.g.,  $N=8$  for 8-bit images), and
- $T_{span}$  = Span of temperature captured in the image.

The radiometric calibration method developed above was segmented into two methods in order to compare temperature measurement accuracies. The first method was referred to as the real-time (RT) radiometric calibration, in which RT image pixels are correlated to RT surface temperatures defined with Equations 1, 2, and 3. Similarly, the second method was termed the one-time (OT) radiometric calibration that utilized one calibration image to determine the radiometric transfer function. The RT radiometric calibration method was developed to test the measurement accuracy of the uncooled TIR cameras where reference temperature panels are consistently viewable within the camera FOV like a fixed platform. On the other hand, the OT radiometric calibration method was developed to test the measurement accuracy of the uncooled TIR camera when reference panels cannot be continuously viewed for practical reasons such as a dynamic sensing platform.

#### *Warm-up Time and Automatic Recalibration*

Uncooled TIR cameras account for microbolometer temperature fluctuations without heavy cooling systems with automatic recalibration. A shutter recalibration technique is activated to conduct a non-uniformity correction (NUC) across the thermal detector at either a user-defined time interval and/or in the event of an internal temperature change of the thermal detector (DRS Technologies, Network and Imaging Systems Group, n.d.). During a NUC, the camera shutter closes to block incoming thermal energy, thereby providing a uniform thermal reference for the detector. At that time, a recalibration algorithm ensures a uniform pixel intensity is measured across the entire microbolometer. Once powered on, an uncooled TIR camera begins to reach a steady state operating temperature as a result of internal circuitry temperature and ambient air conditions.

To determine the amount of time needed to reach the steady state operating temperature from ambient conditions, the TIR cameras were operated in the BB enclosure with steady target temperature for 45 minutes while the video pixel intensities, target surface temperatures, camera housing temperature, and ambient air conditions were monitored. The resulting warm-up time was determined when the measured pixel intensity was within 5% of the stable target pixel intensity.

Because automatic NUC is recommended during regular operation, additional tests were conducted to investigate the influence on temperature measurement accuracy from a 1 min, 5 min, and no NUC. Each test was run for 60 minutes because typical thermography applications occur in a short time span in order to limit time between samples (Maes & Steppe, 2012). Images for these tests were monitored using the DAQ system described above to determine the temperature measurement accuracy under the specific scenarios listed in Table 1.

**Table 1. Non-uniformity correction influence on measurement accuracy ( $\pm^{\circ}\text{C}$ ) with OT and RT radiometric correction**

Video Output	Correction Time		
	No Correction (Sensing Time)	5-minute NUC (Sensing Time)	1-minute NUC (Sensing Time)
Analog	60 minutes	60 minutes	60 minutes
Analog	30 minutes	-	-
Analog	15 minutes	-	-
Digital	60 minutes	60 minutes	60 minutes
Digital	30 minutes	-	-
Digital	15 minutes	-	-

*Connection Ease, Software, and Controllability*

The TIR camera cores provide analog and digital video outputs. Analog output provides an 8-bit (256 discrete pixel intensity DV) thermal video, whereas digital output is 8-bit or 14-bit (256 or 16,384 discrete pixel intensity DV) video. These two modes of video output were investigated in regards to measurement accuracy, temperature resolution (i.e., smallest measurable temperature difference), and ease of image capture regarding necessary hardware and software functionality. Each TIR camera control software’s graphical user interface (GUI) configured the camera for video output and frame rate, user-defined NUC, and thermal detector sensitivity. Although both camera control softwares have distinguishing features, they are not discussed in detail. However, both softwares adjust the thermal detector gain sensitivity (i.e., detectable scene temperature span) and level control (i.e., shift offset of the center temperature within the temperature span), thereby adjusting the slope (m) and level offset (b), respectively, defining a  $y=(m)x+(b)$  format (Figure 5). More specifically, the thermal detector gain sensitivity adjusts the upper and lower pixel saturation and temperature measurement resolution, thereby improving the visibility of desired scene temperatures. For example, a temperature span of 20°C is set by the camera gain control whereas a center temperature of 25°C is controlled by the level control. In this example, the lower and upper saturation temperatures would be at 15°C and 35°C, respectively. In addition, the temperature resolution of the resulting 8-bit image of a 20°C span would equal 0.08°C, as defined by Equation 4:

$$T_{resolution} (^{\circ}\text{C}) = \frac{T_{span} (^{\circ}\text{C})}{2^n} \tag{4}$$

where:

- T<sub>span</sub>=Span of temperatures (°C) measureable by the thermal detector
- N=bits of resolution (e.g., N=8 for 8-bit images), and
- T<sub>resolution</sub>=theoretical temperature resolution

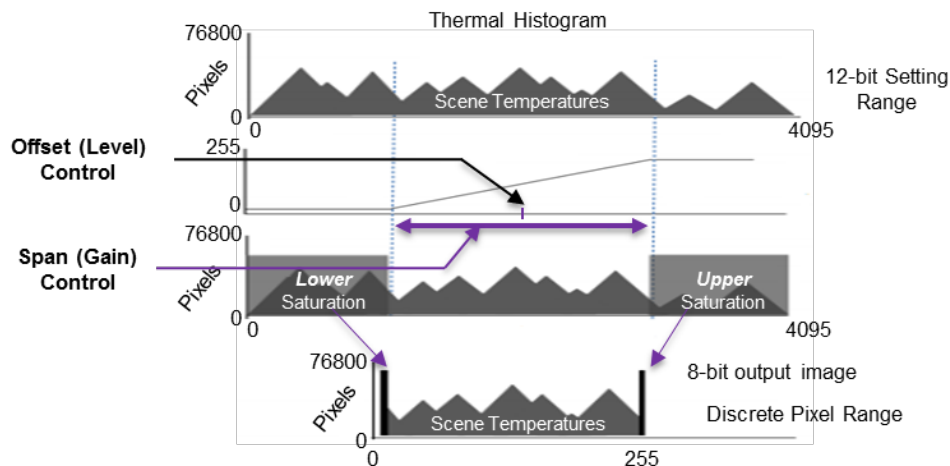


**Figure 5. Camera settings from level and gain control for a thermal detector. The gain control adjusts the thermal detector sensitivity to LWIR energy thereby adjusting the temperature span. Level control adjusts the center offset temperature to adjust the offset of the temperature span. Adapted from DRS Tamarisk® 320 Camera Control Software User Guide (2013).**

A DRS breakout board module (Breakout Box 1003785-001, DRS Technologies, Inc., Dallas, Texas) controlled CAM1 by adjusting the gain and level for the span and center temperature offset. Similarly, CAM2 was controlled via the FLIR® VNC module (FLIR® Systems, Inc., Boston, Massachusetts). Analog video from both uncooled TIR cameras was streamed at 9 Hz into an analog-to-digital video converter (Dazzle DVD Recorder HD, Corel Corporation, USA). This raw analog video signal was streamed into a host computer using LabVIEW™ (National Instruments Corporation, Austin, Texas) image acquisition and processing software that captured, processed, and stored each video frame using a developed virtual interface (VI).

In order to reduce signal loss and noise introduced with analog video signal transmission, digital video feed from CAM1 was captured with an external digital frame grabber (iPORT CL-U3, Pleora Technologies, Ontario, Canada). The frame grabber acquired digital images directly from the TIR camera.

Controllability was studied using digital video feed from CAM1 in order to investigate added functionality (i.e., measurement accuracy, temperature span and resolution) of the digital output configuration. CAM1 was used because the DRS breakout board supported digital video feed while CAM2 required additional breakout boards beyond the FLIR® VNC module.

Using the developed RT and OT radiometric calibration methods described above, the resulting temperature span and offset temperature increment were investigated for each gain and level control setting. In order to determine the temperature span, the aluminum reference target was chilled to 0°C and attached to the heating element held at 65°C. Through convective heat transfer, the aluminum reference target rose from 0°C to 65°C in under 10 minutes. This rise in temperatures were used to determine the thermal detector sensitivity of each TIR camera core under a discrete range of low to high gain settings. In order to determine the level control characteristics, RT pixel intensity of a stable reference temperature was recorded as the camera level control was adjusted from lower to upper pixel saturation for each respective gain setting. With a stable target temperature, the change in the pixel intensity value for each level offset increment was used to characterize the controllability and determine the temperature difference for each level control increment.

### ***Environmental Influence on Measurement Accuracy and Repeatability***

In addition to controlling the heating element, the BB enclosure regulates air exchange within the chamber to pull air from outside the cabinet until equilibrium is automatically or manually reached (Figure 6 b). The BB enclosure was operated within an environmental growth chamber (EGC15, Chagrin, Ohio) in order to investigate the repeatability of the TIR camera under changing environmental conditions (i.e., air temperature and relative humidity) typical in agricultural studies (Figure 6).

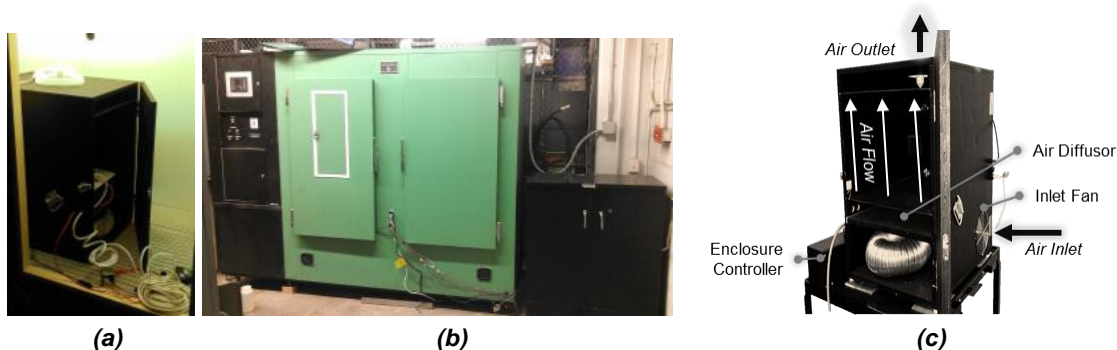


**Figure 6. (a) BB enclosure installed in the (b) environmental chamber for strictly controlled environmental conditions. (c) Air exchange through the BB enclosure controls internal air parameters**

Strict laboratory tests regulated air temperature and relative humidity, providing an evaluation of the measurement accuracy under diverse laboratory conditions (i.e., 15-45°C  $\pm$ 0.3°C, and 25-75%RH  $\pm$ 2.5%). The BB enclosure pulled outside air from the environmental chamber until the set air condition parameters were reached (Figure 6). Eight air temperature namely 10, 15, 20, 25, 30, 35, 40, and 45°C were selected. For each test, the desired air temperature was set while humidity was set at 25% relative humidity. When the specific air conditions were achieved within the BB enclosure, an OT radiometric calibration was performed as the relative humidity on the environmental chamber was set to change from 25% to 75% which occurred over a period of 10 minutes. The change in relative humidity was induced to observe radiant heat attenuation due to increased water vapor between the target and the TIR camera (Monteith & Unsworth, 2013). Environmental attenuation would be consistent between the two camera cores; therefore, only CAM1 was testing in the environmental chamber. An OT radiometric calibration was used because RT radiometric calibration was developed to compensate for changes in ambient conditions.

# Results and Discussion

## Lens Selection and Distortion

The medium angle lens of CAM1 has less visible distortion than the wide angle lens of CAM2 (Figure 7). The wide angle lens (7.5 mm) and medium angle lens (11mm) distortion was 30% and 19%, respectively. However, both distortions were corrected with the resulting lens correction coefficients shown in Table 2. The distortion comparison is not meant to distinguish differences between TIR camera cores, but the difference between medium to wide angle lens focal length and resulting lens FOV degree angle. Distortion coefficients of both camera lenses had to be determined because they were not provided by the TIR camera manufacturer. The results reveal a significant distortion occurs within the germanium lens of each TIR camera core. This will have practical implications where spatial accuracy is critical especially in whole-field temperature mapping and site-specific crop health monitoring. In application, batch image processing would use the resulting lens distortion coefficients within an algorithm in order to undistort images for spatial accuracy for actual location. In addition, since each TIR camera and lens are factory calibrated, a TIR camera and lens combination may have subtle variations in distortion characteristics. As a result, identical camera-lens configurations may not be interchangeable; therefore, each individual TIR camera may need to be calibrated in order to determine specific lens distortion coefficients.

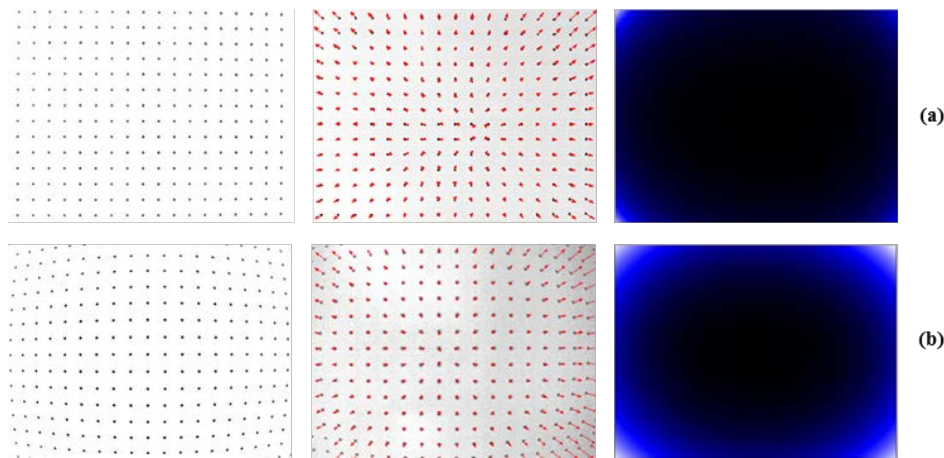


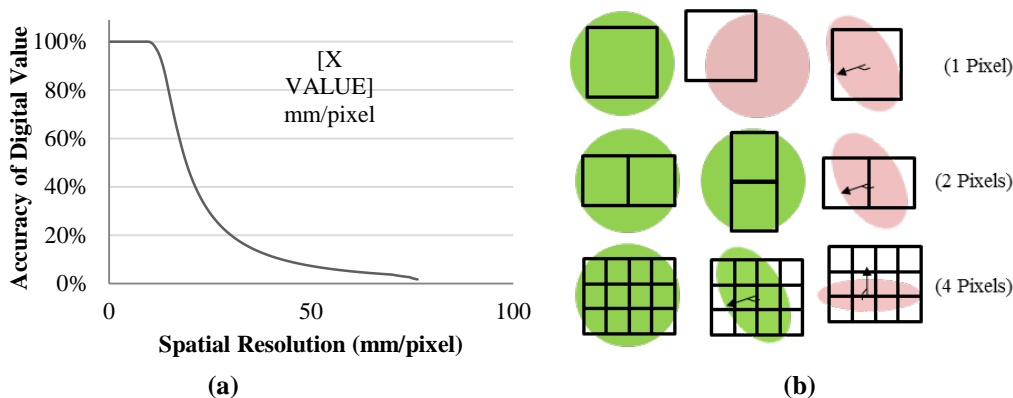
Figure 7. (a) CAM1 with 11 mm and (b) CAM2 with 7.5 mm lens distortion results from the point distortion (grid) model with grid pattern with known point distances (left) point vector map (middle), and visual distortion map (right)

Table 2. Lens distortion results including radial and tangential correction coefficients.

TIR Camera Core	% Distortion	Radial		Tangential	
		$k_1$	$k_2$	$p_1$	$p_2$
CAM1 11 mm lens	19.1	-0.24992	-0.74306	-0.000177	0.002740
CAM2 7.5 mm lens	30.4	-0.43814	0.20181	0.001486	-0.000493

## Image Resolution and Measurement

The increasing pixel-by-pixel-resolution ROI analysis provided necessary spatial resolution to limit false measurements. As shown in Figure 8 a, a 9 mm/pixel spatial resolution was necessary to measure 100% of the DV of the target when the ROI was directly centered on the target normal to the camera. In actual in-field applications, however, a target will seldom be normal to the camera and aligned to the fixed pixel array. Consequently, target orientation and location variation will inherently cause pixels to measure a mixture of background/target temperature (Figure 8 b).



**Figure 8. (a) Spatial resolution versus the digital value accuracy. (b) Generalized pixel orientations and spatial resolutions of 1 pixel, 2 pixel, and 4 pixels incident on a target. Black boxes represent the individual pixel's FOV. Green objects represent an object that can be accurately measured with the pixel orientation and spatial resolution. Pink objects represent an object that is measured with error.**

The first response would be to increase the number of pixels incident on a target by positioning the camera closer. However, this reduces the overall image coverage area and requires a larger volume of images in order to cover the desired ground area at the specific level of detail. For example, 4 pixels on a target, as shown Figure 8 b, better capture a representative value but cannot entirely reduce the inaccuracy from extreme target orientation and shape irregularity (Figure 8 b). At the same time, 4 pixels versus 2 pixels present on a target reduces the overall image coverage area by 75% and requires 4 times the images in order to cover the same surface area. As a result, a tradeoff exists between the coverage area and level of measurable detail possible from a sensing platform. This will be especially important in the case of uncooled TIR camera when the image resolution (i.e., number of pixels in the fixed pixel array) are small compared to typical visible camera image resolutions. This relationship is critical when matching the camera's fixed pixel resolution and lens combination to the necessary spatial resolution because of the volume of data generated in order to achieve the desired application ground coverage and specific level of detail.

### Warm-up Time

The warm-up time for each camera was determined as shown Figure 9. Results show warm-up times of 19 min and 7 min were necessary for CAM1 and CAM2, respectively, in order to reach within 5% of the stable pixel intensity measurement. Timely fluctuations in the first minutes are due to NUC triggered by the change in the thermal detector temperature and/or after the user-defined timed interval of 1 min. During the warmup period, multiple NUC were activated from a temperature change of the microbolometer as shown by the drastic change in measured pixel intensity during the first 5 minutes. Once the camera housing temperature began to level off, less erratic pixel intensities were observed past 5 minutes which may suggest NUC is activated from the timed interval of 1 min rather than the temperature change.

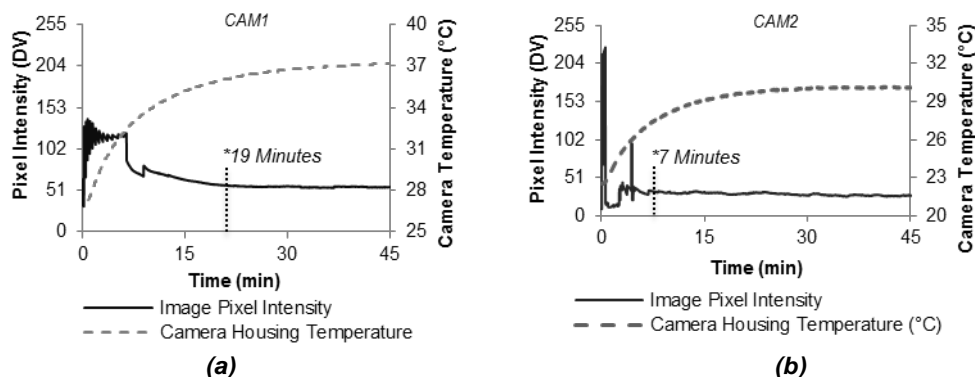


**Figure 9. Raw image intensity and housing temperature versus camera 'on-time' of (a) CAM1 and (b) CAM2. The dotted vertical line indicates the time when measured pixel intensity was within 5% of the stable pixel intensity.**

Prior to the designated warm-up period, inaccuracy exists as the camera reached a stable operating temperature. Camera warm-up time will have implications on how quickly a system can be deployed and is important when considering a standard operating protocol. Furthermore, warm-up time is dependent on the storage temperature prior to operation. In the scenario producing the results shown in Figure 9, the cameras were equal to ambient temperature prior to operation. As a result, warm-up time is dependent on ambient conditions; therefore, allowing TIR cameras to operate beyond the warm-up time will ensure the camera reach a stable operating temperature to

limit inaccurate measurements. In application, starting the camera may be the first step in a standard operating procedure when taking data.

### Radiometric Characterization and Measurement Accuracy

The developed radiometric calibration methods yielded radiometric curves demonstrated in Figure 10. Linear regression analysis showed significant correlation between actual surface temperature and image pixel intensity ( $R^2 = .99$ ) for both TIR camera cores. The resulting linear transfer functions would be directly used to convert image pixel intensities into surface temperature measurements for each camera. Between the two TIR camera cores, the sensitivity to incoming LWIR is comparable. This sensitivity demonstrates uncooled thermal cameras' ability to measure absolute temperatures with additional hardware and software, standard operating protocol for radiometric calibration, and strict camera configurations.

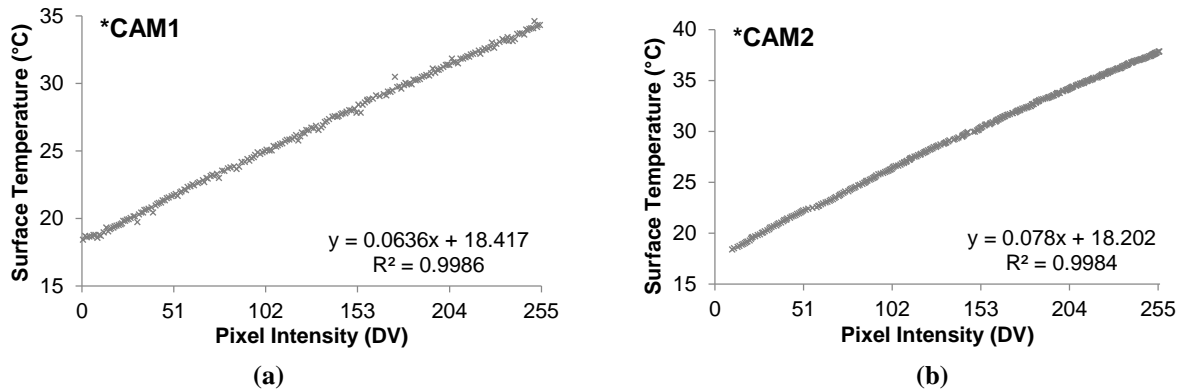


Figure 10. Radiometric calibration performed on the CAM1 (a) and CAM2 (b) at 25°C air temperature and 35% relative humidity after reaching a steady operating temperature.

Because the OT and the RT radiometric calibration methods were developed for different applications, a comparison in Figure 11 shows the measurement accuracy of the two calibration methods. The absolute difference between the actual and measured temperature showed the measurement accuracy was  $\pm 0.38^\circ\text{C}$  or  $0.62^\circ\text{C}$  ( $\alpha=0.05$ ) with RT and OT radiometric calibration, respectively. RT radiometric calibration had a higher measurement accuracy because of the fixed reference panels within the FOV for RT calibration, whereas the same OT radiometric calibration was used throughout the sensing period. As a result, the OT calibration has a diminishing measurement accuracy as the camera continuously conducts a NUC generating slight pixel-to-pixel variation caused by the correction algorithm.

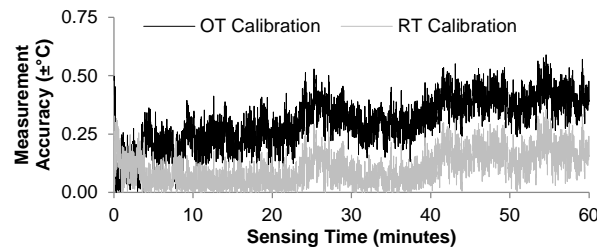


Figure 11. CAM1 measurement accuracy ( $\pm^\circ\text{C}$ ) of OT and RT radiometric calibration process over 1 h. The absolute difference between the actual and measured temperature is shown. CAM1 operated at a stable temperature prior to comparison.

In applications needing a high accuracy with a fixed sensing platform, the RT radiometric calibration would be most applicable. On the other hand, the OT radiometric calibration would be better suited for dynamic sensing platforms in field studies. Most importantly, when considering a TIR camera core and complementary hardware and software, choosing relative versus absolute temperature measurements may reduce the necessary hardware and software, but limit quantifiable temperature measurements. For consistency, the sensing distance was held constant throughout all tests. However, in typical field applications, larger sensing distances beyond that of the BB enclosure may influence the measurement accuracy. As a result, future studies should be conducted that test multiple sensing distances to validate the developed radiometric calibration methods.

### Automatic Recalibration

Because NUC recalibrates the thermal sensor, measurement accuracy with and without NUC is summarized in Table 3. Under operation with and without NUC, measurement accuracy decreased with increased sensing time which is most likely attributed to the slight pixel variation of the NUC. Results showed that a camera configured for a NUC at a user-defined time interval of 1 min yielded the highest measurement accuracy for both analog and digital video systems (Table 3).

However, a RT calibration for a sensing time of 60 min with a 1 min NUC provided similar measurement accuracy as with no NUC with CAM1, thereby suggesting the use of no NUC. However, the strict environmental conditions that produced these results are impractical in agricultural applications. In addition, TIR camera manufacturers do not recommend camera operation without NUC due to potential temperature drift previously discussed. Throughout tests, maximum sensing time used to evaluate the two TIR camera cores was set at 60 minutes. Extended sensing times may need to be investigated for high temporal studies and performance under constant operation.

**Table 3. Measurement accuracy ( $\pm^\circ\text{C}$ ) with OT and RT radiometric correction. (Accuracies shown represent an 95% confidence interval)**

	Video Output	NUC Timed Interval	OT Calibration			RT Calibration		
			15 min	30 min	60 min	15 min	30 min	60 min
CAM2	Analog	1 min	-	-	0.87	-	-	0.63
		5 min	-	-	1.00	-	-	0.72
		<sup>[a]</sup> W/O	0.67	0.80	0.92	0.47	0.53	0.74
CAM1	Analog	1 min	-	-	0.82	-	-	0.62
		5 min	-	-	1.15	-	-	0.65
		<sup>[a]</sup> W/O	0.60	0.73	0.87	0.38	0.49	0.62
	Digital	1 min	-	-	0.43	-	-	0.29
		5 min	-	-	0.95	-	-	0.54
		<sup>[a]</sup> W/O	0.30	0.35	0.64	0.29	0.30	0.35

<sup>[a]</sup> Subject to thermal detector sensor drift from internal and external temperature inaccuracy. Not recommended from TIR camera manufacturer

### Connection Ease, Software, and Controllability

Required evaluation hardware for analog video capture was enabled with off-the-shelf (OTS) equipment with camera control software from TIR manufacturers for full evaluation of camera controls and features. As observed, manual control of the thermal detector through the camera control software with radiometric calibrations revealed the characteristic linear transfer functions of gain and level controls, as shown in Figure 12 and Figure 13. This knowledge is important in order to set the cameras for a particular temperature span and offset the center temperature. As observed, a configured temperature span has a direct influence on the discrete temperature resolution measurable from the thermal detector. As a result, the ability to set a specific temperature span could result in the ability in order to better assess discrete spatial crop temperature differences.

For application in crop sensing, a minimum temperature resolution of  $0.5^\circ\text{C}$  is suggested to measure the subtle temperature differences for crop health assessment (Sepulcre-Canto, et al., 2007). As a result, a limitation of the 8-bit image data is the coarse temperature resolution with large temperature spans. As shown in Table 4, the minimum temperature resolution suggested by Sepulcre-Canto et al. (2007) of  $0.5^\circ\text{C}$  would result in a temperature span close to  $120^\circ\text{C}$ . In order to cover twice the suggested temperature resolution, a minimum temperature resolution of  $0.25^\circ\text{C}$  was chosen to determine the maximum temperature span ( $60^\circ\text{C}$ ) in Figures 12 and 13.

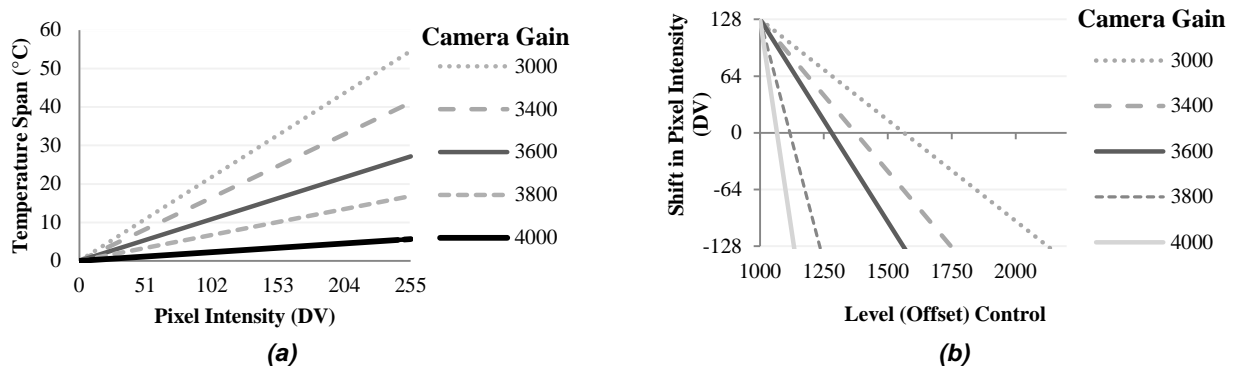


Figure 12. CAM1 camera (a) gain for temperature span and (b) level setting characteristics for offset temperature bias.

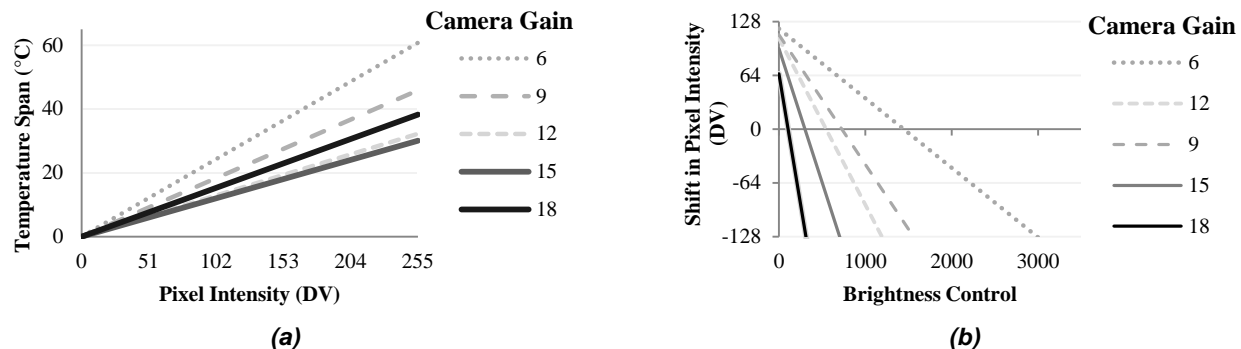


Figure 13. CAM2 camera (a) gain for temperature span and (b) level setting characteristics for offset temperature bias.

With Equation 4, Table 4 demonstrates theoretical temperature resolution of selected temperature spans of the analog and digital output. By using Equation 4, digital output from CAM1 resulted in a fixed temperature span of 156°C with a fixed 0.01°C temperature resolution. Similarly, analog output from CAM1 resulted in a configurable temperature span from 5°C to 156°C and resolution from 0.02°C to 0.61°C. Analog output from CAM2 yielded a controllable temperature span of 18°C to 206°C and resolution of 0.07°C to 0.80°C.

Table 4. Temperature resolution (°C) of specific temperature span

Video Type (bits)	Span (°C)							
	<sup>[a]</sup> 200	150	100	50	40	30	20	10
Analog (256)	0.78	0.59	0.39	0.20	0.16	0.12	0.08	0.04
Digital (16,384)	-	0.01	<sup>[b]</sup> 0.01					

<sup>[a]</sup> Only the FLIR® Tau 2 (324) is sensitive to a temperature span of 200°C

<sup>[b]</sup> Based on fixed temperature span and resolution of the digital output

Results in Table 4 will have implications on a sensing application that requires a large temperature span and high temperature resolution. Therefore, a digital output would provide the full temperature span and resolution of the thermal detectors. In addition, TIR cameras have a low signal-to-noise ratio that neither digital nor analog video equipment can reduce. However, digital video hardware eliminated noise introduced with analog video transmission while streaming 14-bit video data.

### Environment Influence

Due to the unregulated temperature of the microbolometer, a change in thermal detector temperature during the warm-up period caused a decrease in measurement inaccuracy (Figure 11, above). Similarly, evaluation within the environmental chamber revealed a change in ambient air temperature caused a proportional change in camera housing temperature, thereby causing similar measurement inaccuracy (Figure 14).

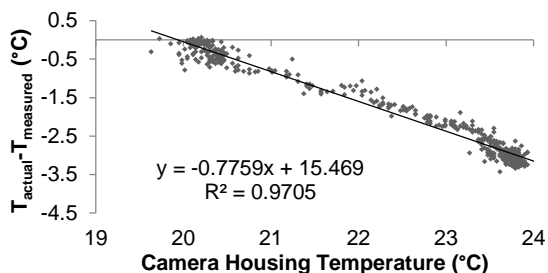


Figure 14. Measurement inaccuracy due to a change in camera housing temperature over a 10 min time span. OT radiometric calibration was performed when the TIR camera housing was at 20°C. CAM1 was configured for 1 min NUC, analog video output and a temperature span of 20°C. Ambient air temperature was 10°C and relative humidity was 25%. CAM1 operated at a stable temperature prior to inducing a change in ambient air temperature.

As camera housing temperature increased, the measured temperature was consistently higher than the actual temperature. This consistent temperature increase could be attributed to how the microbolometer quantifies a pixel intensity due to a change in resistance of an individual pixel detector. As the camera housing temperature increases, the heat transfer to the microbolometer would cause individual pixel resistances to increase resulting in a higher measured temperature. Results from an increased relative humidity was investigated and the resulting influence to measurement accuracy is shown in Figure 15. As shown in Figure 15 a, a target with a stable temperature above air temperature resulted in a decreased measured temperature that appeared to attenuate towards ambient air temperature with increasing relative humidity. Similarly, a target with a stable temperature below air temperature (Figure 15 c) resulted in an increased measured temperature that appeared to attenuate towards ambient air temperature with increasing relative humidity. Lastly, a target with a stable temperature equal to air temperature (Figure 15 b) resulted in a measured temperature that remained closely centered to air

temperature but with diminished accuracy. With stable targets not equal to air temperature, the apparent attenuation towards ambient air temperature is most likely due to ambient air particles in-between the target surface and camera. In the scenario with the stable target equal to air temperature, some inaccuracy may be contributed to air particles that are not in equilibrium with the ambient air, thereby causing the apparent decrease in measurement accuracy.

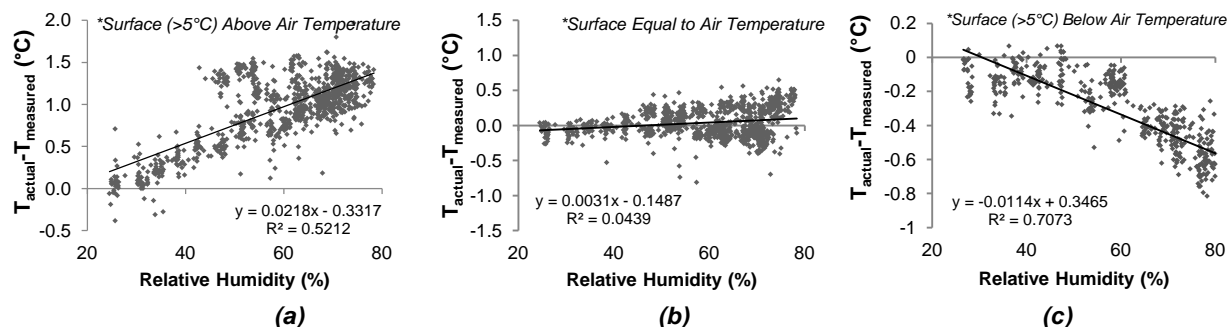


Figure 15. Influence of relative humidity changes to measurement accuracy between the TIR camera and the stable target whose temperature is (a) above (>5°C) ambient air temperature, (b) equal to air temperature, and (c) below (>5°C) air temperature. CAM1 was configured for 1 min NUC, analog video output, and a temperature span of 20°C. CAM1 operated at a stable temperature prior to the inducing a change in relative humidity.

Results indicate air temperature and relative humidity can impact measurement accuracy of the TIR camera systems. The  $R^2$  values for plots in Figure 14 and 15 indicated that regression curves can be generated to compensate for temperature and humidity changes. However, further research needs to be conducted to understand these affects with the TIR camera system at different sensing distances especially aboard sUAS platforms.

To account for changing environmental conditions, an OT radiometric calibration at a specific air temperature, relative humidity, and camera housing temperature produced an accurate surface temperature measurement (Figure 16). Similarly, a RT radiometric calibration maintained measurement accuracy from changing environmental conditions. Depending on the application, the OT radiometric calibration method may be appropriate if conditions such as air temperature, relative humidity, and camera thermal detector temperature go unchanged, while the RT calibration accounts for the instantaneous environmental conditions.

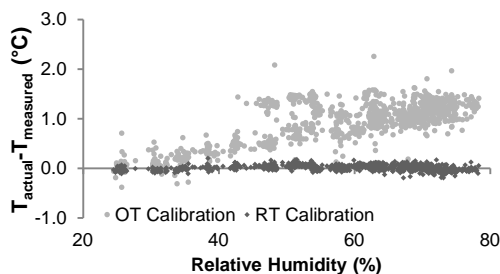


Figure 16. RT versus OT radiometric calibration under changing relative humidity. OT radiometric calibration was conducted when chamber was at a relative humidity of 25%. CAM1 was configured for 1 min NUC, analog video output, and a temperature span of 20°C. CAM1 operated at a stable temperature prior to the inducing a change in relative humidity.

Further studies should be conducted with TIR camera cores within semi-regulated and unregulated environmental settings in order to fully investigate TIR camera core utility and the robustness of the developed calibration methods in dynamic field operations.

## Conclusion

Uncooled TIR camera core evaluations were conducted to answer questions on use and standard operating protocol, system complexity, and measurement accuracy in changing environmental conditions, which has restricted previous use. More specifically, this study determined the necessary hardware and influences to measurement accuracy from physical properties and some environmental conditions present in agricultural applications. As studied, physical properties that reduce practical use of TIR cameras for temperature measurement include lens distortion, image pixel resolution, warm-up time, camera controllability, and repeatability. However, negative influences on measurement accuracy can be reduced with camera configuration

settings, a camera-lens combination selected for sensing distance and target dimensions, post-processing lens calibrations, and standard operating protocol.

In this study, the wide angle lens (7.5 mm) and medium angle lens (11mm) distortion was 30% and 19%, respectively, that image distortion correction resolved for precise spatial integrity. At least 4 pixels are recommended on the target in order to capture a representative value from the target and maximize the image coverage area while accounting for slight inconsistencies in target orientation and shape. Warm-up times of 7 and 19 min are necessary for a stable temperature measurement of CAM2 and CAM1, respectively. With a 1 min timed-interval NUC over a sensing period of 1 h, OT or RT radiometric calibration provided absolute surface temperatures with environmental compensation in which the TIR camera was calibrated. The CAM1 analog output yielded a configurable temperature span from 5°C to 156°C, resolution from 0.02°C to 0.61°C, and measurement accuracy of  $\pm 0.82^\circ\text{C}$  or  $0.62^\circ\text{C}$  with OT or RT radiometric calibration, respectively. CAM 1 digital output yielded a fixed temperature span of 156°C, resolution of 0.01°C and measurement accuracy of  $\pm 0.43$  or  $0.29^\circ\text{C}$  with OT or RT radiometric calibration, respectively. CAM2 yielded a controllable temperature span of 18°C to 206°C, resolution of 0.07°C to 0.80°C, and measurement accuracy of  $\pm 0.87$  or  $0.63^\circ\text{C}$  with OT or RT radiometric calibration, respectively. Both TIR camera cores had a thermal detector that was sensitive and directly correlated to the temperature within the FOV ( $R^2 = 0.99$ ), thereby resulting in comparable measurement accuracies between the two TIR cameras.

Increased measurement temperature accuracy, resolution, and added control was achieved by integrating a digital frame grabber to reduce analog signal loss and noise introduced with analog video signal transmission. The DRS Breakout Box in conjunction with CAM1 was advantageous because it acts as the analog and digital module while doubling as the control interface. Both cameras were configurable for a span of temperatures, but CAM1 had more discrete settings in order to make fine adjustments to span and offset temperature.

Findings of this research support future studies to capture spatial temperatures aboard ground and aerial-based sensing platforms to generate high-spatial thermal images for unique monitoring of crop health for new and advanced relationships.

## Acknowledgements

A special acknowledgement and great appreciation is extended to DRS Technologies, Inc. for their assistance in providing a TIR camera core as well as on-going support throughout the research. Similarly, support for hardware and software was provided by the Biological and Agricultural Engineering Department with guidance and support from Dr. Ajay Sharda, Dr. Naiqian Zhang, and Jonathan Zeller.

## References

- Adeuya, R., 2007. Improving Agricultural Sustainability through drainage water management practices.. *Grants and Education to advance innovations in sustainable agriculture*, Volume GNV06-066.
- Berni, J. A. et al., 2009. Mapping canopy conductance and CWSI in olive orchards using high resolution thermal remote sensing imagery. *Remote Sensing of Environment*, pp. 2380-2388.
- Berni, J. A., Zarco-Tejada, P. J., Suarez, L. & Fereres, E., 2009. Thermal and narrowband multispectral remote sensing for vegetation monitoring from an. *IEEE Transactions on Geoscience and Remote Sensing*, March, 47(3).
- Berton, V., 2006. Smart water use on your farm or ranch. *Sustainable agriculture network*, pp. 12-15.
- Blonquist, M. & Bugbee, B., n.d. *Measuring Crop Water Stress Index: Empirical Versus Theoretical Approaches*, s.l.: Apogee Instruments.
- DRS Technologies A Finmeccanica Company, 2013. *Tamarisk 320 Camera Control Software User Guide*. E ed. Dallas, TX: s.n.
- DRS Technologies, Network and Imaging Systems Group, n.d. *Benefits of a thermal camera shutter*, Dallas, TX: DRS Technologies.
- Ehrler, W. L., 1973. Cotton leaf temperatures as related to soil-water depletion and meteorological factors. *Agronomy Journal*, Volume 65, pp. 404-409.
- Elfaki, M. S., Zhang, N. & Peterson, D. E., 2000. Factors affecting color-based weed detection. *Transactions of the ASAE*, Volume 43, pp. 1001-1009.
- Evans, D. E., Sadler, E. J., Camp, C. R. & Millen, J. A., 2000. *Spatial canopy temperature measurements using center pivot mounted IRTS*. Madison, WI, s.n.
- Fitzgerald, G. J. et al., 2007. Spectral and thermal sensing for nitrogen and water status in rainfed and irrigated wheat environments. *Precision Agriculture*, Volume 7, pp. 233-248.
- Gomide, R. L., Tian, L. & Pinto, F., 2003. *Thermal and color near-infrared spectral remotely sensed scanners to detect in-field soybean and corn water stress variability*., Las Vegas: s.n.
- Grant, O. M., Tronina, L., Jones, H. G. & Chaves, M. M., 2007. Exploring thermal imaging variables for the detection of stress responses in grapevine under different irrigation regimes. *Journal of Experimental Botany*, 58(4), pp. 815-825.
- Hashimoto, Y. et al., 1984. Dynamic Analysis of Water Stress of Sunflower Leaves by Means of a Thermal Image Processing System. *Plant Physiology*, Volume 76, pp. 266-269.
- Herwitz, S. R. et al., 2004. Imaging from an unmanned aerial vehicle: agricultural surveillance and decision support. *Computers and Electronics in Agriculture*, Volume 44, pp. 49-61.
- Idso, S. B., Jackson, R. D. & Reginato, R. J., 1977. Remote sensing of crop yields. *Science*, Volume 196, pp. 19-25.
- Jones, H. G., 2004. Irrigation scheduling: advantages and pitfalls of plant-based methods. *Journal of Experimental Botany*, Volume 55, pp. 2427-2436.
- Kuenzer, C., 2014. *Thermal Infrared Remote Sensing: Sensor, Methods, Applications*. New York(New York): Springer.
- Laguela, S., Diaz-Vilarino, L., Roca, D. & Armesto, J., 2013. *Aerial thermography from low-cost UAV for the generation of thermographic digital terrain models*, University of Vigo: s.n.
- Leinonen, I. & Jones, H. G., 2004. Combining thermal and visible imagery for estimating canopy temperature and identifying plant stress. *Journal of Experimental Botany*, June, 55(401), pp. 1423-1431.
- Liu, Y. et al., 2011. Maize leaf temperature responses to drought: thermal imaging and quantitative trait loci (QTL) mapping. *Environmental and Experimental Botany*, Volume 71, pp. 158-165.
- Sepulcre-Canto, G. F. et al., 2011. Estimating crop-specific evapotranspiration using remote sensing imagery at various spatial resolutions for improving crop growth modelling.. *International Journal of Remote Sensing*, 34(9-10), pp. 3274-3288.
- Sepulcre-Canto, G. et al., 2007. Monitoring yield and fruit quality parameters in open canopy tree crops under water stress.. *Remote Sensing of Environment*, Volume 107, pp. 455-470.
- Taghvaeian, S. et al., 2013. Minimizing instrumentation requirement for estimating crop water stress index and transpiration of maize. *Irrigation Science*.

Taghvaeian, S. et al., 2013. Remote sensing for evaluating crop water stress at field scale using infrared thermography: potential and limitations. *Hydrology Days*, pp. 73-83.

The Mathworks, Inc., 2015. *Developing an algorithm to undistort pixel locations of an image*, s.l.: Mathworks.

USDA, 2014. *Irrigation and Water Use*. [Online]  
Available at: <http://www.ers.usda.gov/topics/farm-practices-management/irrigation-water-use.aspx#.UyfBjUlotW>

Zhang, C. & Kovacs, J. M., 2012. The application of small unmanned aerial systems for precision agriculture:a review. *Precision Agriculture*, 2012(13), pp. 690-712.